Synthesis, Crystal Structure, Electronic Structure, and Properties of Hf_2In_5, a Metallic Hafnide with One-Dimensional Hf–Hf and Two-Dimensional In–In Bonding

Rainer Pöttgen* and Richard Dronskowski*

Abstract: Hf_2In_5—previously reported with the tentative composition "Hf_3In_4"—was prepared from the elements in a tantalum tube at 970 K. The X-ray diffractional characterization by means of single-crystal refinement reveals the presence of a tetragonal structure ($a = 1024.71(9)$, $c = 305.66(3)$ pm, *P4/mbm*, $Z = 2$) of Mn_2Hg_5 type. Hf_2In_5 is Pauli-paramagnetic and a good metallic conductor. Quasi-relativistic semiempirical and scalar-relativistic ab initio band structure calculations reveal Hf_2In_5 to be a hafnide, composed of a two-dimensional indium network threaded by infinite hafnium chains. The amount of In–In bonding scales counterintuitively with the interatomic distances.

Keywords
crystal structure · electronic structure · hafnium compounds · indium compounds · metallic conductivity

Introduction

At the present time, the solid-state chemistry of indium is experiencing a true renaissance. Current research has mainly focused on two challenging subjects. First, numerous recent investigations by the groups of Corbett and Cordier (ref. [1–8], and ref. therein) in the field of binary alkali metal–indium compounds and their ternary substitution variants have led to the generation of novel indium cluster materials with an astonishing structural variety. The latter are characterized by complex multibonding phenomena. Ever since the early work of Thümmel and Klemm,[9] the structural and physical properties of this type of compound have proven to be worthwhile subjects of research. Second, there is a growing number of reduced binary and ternary indium halides in which monovalent indium, because of its unusual electronic state, is the source of uncommon chemical and physical effects. For example, these compounds are known to be highly sensitive to physical manipulation (air, humidity, pressure, light, etc.) and highly reactive in the solid state towards organic molecules, and the atomic sites show second-order Jahn–Teller instabilities (ref. [10–13], and ref. therein).

When it comes to the structural characterization of binary *transition metal* indium phases, however, our knowledge is very limited. In fact, although many analytical investigations on such phases have been carried out within the last thirty years,[14, 15] surprisingly little information on their crystal structures and physical properties is available. We have therefore recently started more systematic studies into these compounds, and we have already reported the crystal structures and physical properties of $RuIn_3$[16] and Ti_2In_5;[17] the latter had previously been assigned the tentative composition "Ti_3In_4".[18, 19] Since an analogous phase with an approximate composition "Hf_3In_4" had also been observed[19] in the hafnium–indium binary system (up to then the highest proportion of indium reported in a binary hafnium compound), we also reinvestigated this phase. Our studies on a single crystal show the correct composition to be Hf_2In_5, paralleling the results obtained previously for Ti_2In_5.[17] This, and our investigations into the magnetic properties, electrical properties, and chemical bonding in Hf_2In_5, are reported in the present paper.

[*] Dr. R. Pöttgen,[+] Priv.-Doz. Dr. R. Dronskowski
Max-Planck-Institut für Festkörperforschung
Heisenbergstrasse 1, 70569 Stuttgart (Germany)
e-mail: drons@simix.mpi-stuttgart.mpg.de

[+] New address: Anorganisch-Chemisches Institut, Universität Münster
Wilhelm-Klemm-Strasse 8, 48149 Münster (Germany)
Fax: Int. code +(251)83-3136
e-mail: pottgen@VNWZ00.uni-muenster.de

Experimental Procedure and Theoretical Techniques

Synthesis: Starting materials for the preparation of Hf_2In_5 were hafnium shot (80–200 mesh, Johnson Matthey, >99.5%) and indium tear drops (Johnson Matthey, >99.9%). The elements were mixed in the ideal atomic ratio and sealed in a tantalum tube under an argon pressure of about 800 mbar. The argon had previously been purified over molecular sieves, titanium sponge (at 900 K), and an oxisorb catalyst [20]. The tantalum tube was sealed in a quartz glass ampoule to prevent oxidation. It was first heated at 1320 K for two days, and the temperature was then decreased in steps of 50 K (every two days), and at 970 K the sample was annealed for three more weeks. The long annealing times were needed in order to increase the sample quality and the crystal size. In contrast, microcrystalline single phase Ti_2In_5 [17] samples could already be synthesized overnight.

Crystal-Structure Analysis: The isotypism of Hf_2In_5 with Ti_2In_5 showed up from modified Guinier powder patterns [21], which were recorded with Cu $K\alpha_1$ radiation with 5N silicon ($a = 543.07$ pm) as an internal standard. The patterns were indexed on the basis of a tetragonal cell with the lattice constants given in Table 1. The correct indexing was then assured by intensity calculations [22] taking the atomic positions from the structure refinement. Needle-shaped single crystals were isolated from the annealed sample by mechanical fragmentation and were examined with a Buerger precession camera in order to establish both symmetry and suitability for intensity-data collection. The precession photographs showed the presence of tetragonal symmetry, and the systematic extinctions were compatible with space group *P4/mbm* (no. 127), in agreement with the previous investigation on the titani-

0947-6539/96/0207-0800 $ 15.00+.25/0

Table 1. Crystallographic data for Hf_2In_5.

formula; M_r	Hf_2In_5; 931.08 g mol^{-1}
T	293(2) K
space group; formula units	$P4/mbm$, D_{4h}^5 (no. 127); $Z = 2$
unit cell dimensions	$a = 1024.71(9)$, $c = 305.66(3)$ pm
(Guinier powder data)	$V = 0.32095(5)$ nm^3
X-ray density; $F(000)$	9.634 g cm^{-3}; 778
crystal size	$10 \times 10 \times 80$ μm^3
instrument	Enraf-Nonius CAD4 four-circle diffractometer, $Ag_{K\alpha}$, graphite monochromator, scintillation counter
absorption correction	from ψ-scan data; 10 reflections
transmission ratio (max:min)	0.979:0.724
absorption coefficient	26.58 mm^{-1}
scan range; type	$2 \le \theta \le 25°$; ω/θ scan
scan speed	variable, prescan-dependent
range in hkl	$0 \le h \le 12$, $-12 \le k \le 15$, $-4 \le l \le 4$
total no. reflections	1513
independent reflections	354 ($R_{int} = 0.0569$)
reflections with $I > 2\sigma(I)$	322 ($R_{sigma} = 0.0361$)
refinement method	full-matrix least-squares on F^2
data/restraints/parameters	353/0/15
goodness-of-fit on F^2	1.256
final R indices [$I > 2\sigma(I)$]	$R1 = 0.0248$, $wR2 = 0.0467$
R indices (all data)	$R1 = 0.0298$, $wR2 = 0.0485$
extinction coefficient	0.0141(8)
largest diff. peak and hole	1363 and −1821 e nm^{-3}

um compound [17]. Relevant crystallographic data and details of the data collection are listed in Table 1. The positional parameters of Ti_2In_5 [17] were taken as starting values and the structure was successfully refined using SHELXL-93 [23] with anisotropic displacement parameters for all atoms. A final difference Fourier synthesis revealed no significant residual peaks. Table 2 shows positional and isotropic diplacement parameters, as well as anisotropic displacement parameters; the latter are very well behaved. Table 3 gives selected interatomic distances [24].

Table 2. Atomic coordinates and anisotropic displacement parameters (pm^2) for Hf_2In_5. U_{eq} is defined as one third of the trace of the orthogonalized U_{ij} tensor. The anisotropic displacement factor exponent takes the form: $-2\pi^2[(ha^*)^2 U_{11} + \ldots + 2hka^*b^*U_{12}]$. ($U_{13} = U_{23} = 0$).

	Wyckoff position	x	y	z	U_{eq}
Hf	4*h*	0.18029(3)	$^1/_2 + x$	$^1/_2$	67(2)
In(1)	2*d*	0	$^1/_2$	0	87(3)
In(2)	8*i*	0.06116(6)	0.20765(6)	0	92(2)
	U_{11}	U_{22}	U_{33}	U_{12}	
Hf	67(2)	U_{11}	66(2)	−3(2)	
In(1)	86(4)	U_{11}	90(5)	−42(4)	
In(2)	65(3)	117(3)	94(3)	23(2)	

Table 3. Interatomic distances (pm) in the structure of Hf_2In_5. All distances shorter than 520 pm (Hf–Hf), 485 pm (Hf–In), and 430 pm (In–In) are listed. The standard deviations are all equal to or less than 0.1 pm.

Hf	–In(1)	302.7 (2×)	In(2)	–In(2)	305.7 (2×)
	–Hf	305.7 (2×)		–In(1)	306.1
	–In(2)	307.1 (4×)		–Hf	307.1 (2×)
	–In(2)	312.7 (4×)		–Hf	312.7 (2×)
				–In(2)	313.7 (2×)
In(1)	–Hf	302.7 (4×)		–In(2)	335.0
	–In(1)	305.7 (2×)			
	–In(2)	306.1 (4×)			

Band-Structure Calculations: The electronic-structure calculations of Hf_2In_5 were performed at two different levels of sophistication. Semiempirical tight-binding calculations helped in the analysis of chemical bonding, whereas ab initio computations were needed for the generation of charge density plots. A comparison between both approaches was attempted in order to estimate the quality of the semiempirical method. All computations were carried out on a DECstation 5000/133 machine, running under the UNIX operating system.

Semiempirical Calculations: The quasi-relativistic band-structure calculations (EH-TB) were essentially based on an extended Hückel hamiltonian [25,26], whereas off-site hamiltonian matrix elements were evaluated according to the weighted Wolfsberg–Helmholz formula [27], minimizing counterintuitive orbital mixing. The minimal orbital basis set was composed of Slater orbitals that had been scaled to j-averaged values of numerical Dirac–Fock atomic functions; also, on-site hamiltonian matrix elements were approximated by averaged atomic orbital energies from the same source [28,29]. In detail, the exchange integrals were (ζ orbital exponents in parentheses): Hf 6s, −6.52 eV (1.673); Hf 6p, −3.75 eV (1.141); In 5s, −10.79 eV (2.023); In 5p, −5.35 eV (1.367). To obtain greater accuracy, the Hf 5d atomic wavefunction (average orbital energy −6.57 eV) was approximated by a double zeta function with exponents $\zeta_1 = 3.337$ and $\zeta_2 = 1.505$, and weighting coefficients $c_1 = 0.637$ and $c_2 = 0.546$. The eigenvalue problem was solved in reciprocal space at 110 k points within the irreducible wedge of the brillouin zone, by using a modified EHMACC code [30].

Ab Initio Calculations: Scalar relativistic electronic structure calculations of ab initio quality including mass-velocity and Darwin terms were performed using LMTO (linear muffin-tin orbital) theory [31–34], a fast linearized form of the KKR method [35,36]. The method accounts for the potential from all the electrons and is applicable to materials composed of atoms from any part of the periodic table. Its almost minimal, unfixed basis sets adjust dynamically to the respective potentials. In the interstitial regions with flat potentials, the wave functions of the valence electrons are expanded into Hankel envelope functions, whereas in the corelike regions one seeks numerical solutions of the radial Schrödinger equation. For Hf_2In_5, the electronic energy was computed with the help of density-functional theory, replacing the many-particle problem by the self-consistent solution of the Kohn–Sham equations [37,38], taking the von Barth and Hedin parametrization [39].
A minimal basis set of short-range atom-centered TB-LMTO's was used [40], which has one s, three p, five d, and seven f orbitals on each of the atoms. Hafnium f and indium df orbitals were included by using a downfolding technique. Six additional "empty spheres" (atomic wave functions without nuclei) per cell were introduced in order to reduce interatomic overlap and to improve variational freedom. Starting from Hartree potentials, the structure was iterated by use of the atomic-spheres approximation (ASA), employing muffin-tin spheres expanded to overlapping and volume filling spheres (including a combined correction term). The integration in k space was performed with the help of an improved tetrahedron method [41] using 110 inequivalent k points and 720 different tetrahedra. With this setting, the convergence was better than 2 meV. After having reached self-consistency, charge density plots were generated upon switching to full-potential LMTO mode, dropping any shape approximations for the charge density. The program used corresponds to the TB-LMTO 4.6 code [42].

Magnetic Measurements: A polycrystalline 131.5 mg sample of Hf_2In_5 was subjected to a susceptibility measurement by use of a Quantum Design MPMS SQUID magnetometer within a temperature range of 4.2–300 K at a magnetic flux density of 1 T.

Electrical Conductivity: Resistivity measurements were performed on a small block ($0.8 \times 1.4 \times 1.7$ mm^3, cut with a diamond saw from a larger ingot) in a conventional four-probe setup. Cooling and heating curves taken at a constant current between 4.2 and 300 K were essentially identical in size and shape.

Results and Discussion

Geometric and Electronic Structure: The composition Hf_2In_5 can be deduced unambiguously from the quantitative synthesis as well as from the present single-crystal investigation. It is clear now that the formerly described phase "Hf_3In_4" of Raman and Schubert[19] is identical with the present compound, as can also be judged from the previously published lattice constants of "Hf_3In_4" ($a = 1023$, $c = 305.3$ pm) derived from powder data. Indeed, Raman and Schubert had proposed the correct lattice sites, however, their atomic assignment (Hf) of the 2*d* position (Table 2) must be changed to indium. Thus, Hf_2In_5 adopts the Mn_2Hg_5 structure type,[43] as does isotypic Ti_2In_5.[17] A perspective view of the Hf_2In_5 structure is shown in Figure 1. Topologically, the indium atoms form planar layers (3.5.4.5 nets) at $z = 0$, which may be described as a tessellation of triangles, squares, and pentagons. The hafnium atoms, at $z = {}^1/_2$, occupy the large pentagonal prismatic voids, while all quadratic and trigonal prisms remain empty.

The density-of-states (DOS) curves of Hf_2In_5 are given in Figure 2, with the local hafnium contributions emphasized in

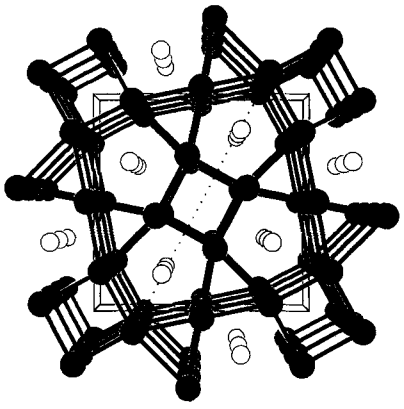

Fig. 1. Perspective view of the tetragonal Hf_2In_5 structure along the z axis. The indium atoms are shown as filled circles and the hafnium atoms as open circles. The dashed line indicates the cut for the charge-density analysis in Figure 6b.

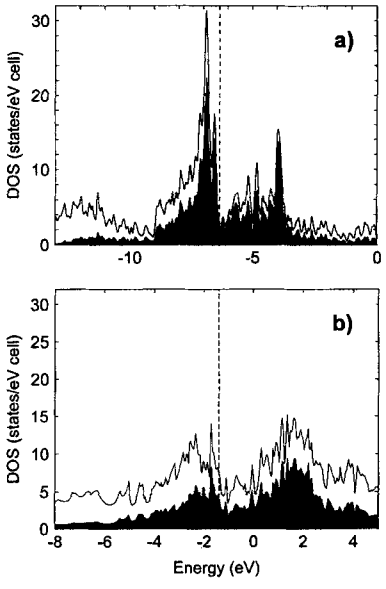

Fig. 2. a) Semiempirical (EH-TB) and b) ab initio (TB-LMTO-ASA) density-of-states (DOS) of Hf_2In_5 with Hf contributions emphasized in black. The Fermi level is given as a dashed line, and both energy ranges cover 13 eV. Note that, because Bloch's theorem was used, the difference in energy zeros is fully irrelevant.

black. Both semiempirical (a) and ab initio calculations (b) reveal the material as being metallic with a nonvanishing DOS at the Fermi level (dashed line). Also, the frontier bands are dominated by hafnium levels more strongly in the semiempirical than in the ab initio calculation. There are two main oversimplifications in the extended Hückel scheme, compared to the ab initio calculation: 1) The d levels that are very close to the Fermi level are too strongly spiked, owing to an insufficient s/d mixing on the hafnium atom; 2) as mentioned above, there is significantly more indium character in the frontier bands of the LMTO DOS, suggesting that interatomic mixing is also underestimated in the semiempirical calculation. The overall shapes of the valence DOS (wide s background, d splitting around the Fermi level ε_F, reduced DOS at ε_F), however, are similar in both descriptions.

It is interesting to note that atomic charges derived from the (semiempirical) Mulliken population analysis (Hf: −1.056; In: +0.422) reveal that, with respect to the elements, electron density has moved from indium to hafnium. A charge transfer might have been predicted based on the absolute electronegativities of Hf (3.80 eV) and In (3.10 eV), as given by Pearson.[44] In contrast, most alkali metal–indium compounds have been described as indides, containing negatively charged indium (clusters).[1–8]

In Figure 3, we take a closer look at the specific coordination of the hafnium atom. The Hf coordination number (CN) is twelve—ten indium neighbors form the pentagonal prism, and two additional hafnium atoms are situated above and below the prism. The average Hf–In distance (308 pm) neither coincides with the sum of the covalent radii (294 pm[45]), nor with the sum of the metallic radii (324 pm[46]); this nicely reflects the partial ionic character of the bonding mentioned above. The Hf–Hf distance (identical with the c lattice parameter) of 306 pm, on the other hand, is 10 pm shorter than the average metal–metal distance in metallic, hexagonal close-packed hafnium.[47] We have to admit, of course, that such a simple comparison of the interatomic distances with these radii is not completely justified, since the differences in coordinations (non-close-packed structure) and the non-isotropic chemical bonding (see below) would have to be considered classically here.

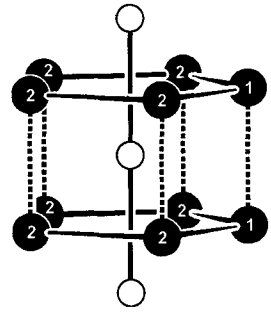

Fig. 3. Coordination polyhedron of the hafnium atoms in Hf_2In_5.

Both indium positions have CN 10, with four hafnium and six indium atoms in their coordination shells. The average In(1)–In and In(2)–In distances of 306 and 313 pm are significantly shorter than the average In–In distance of 334 pm for the twelve nearest neighbors in elemental indium.[47] However, they are only about 10 pm longer than the covalent single-bond length of 299 pm according to Pauling.[45] Similar In–In distances are typically observed in the indium clusters of the binary alkali metal–indium compounds.[1–8]

Figure 4 (left), showing the ab initio band structure of Hf_2In_5, allows access to the spatially resolved bonding in reciprocal space. The progression of the bands may be understood by referring to the primitive tetragonal Brillouin zone sketched in Figure 4 (right).

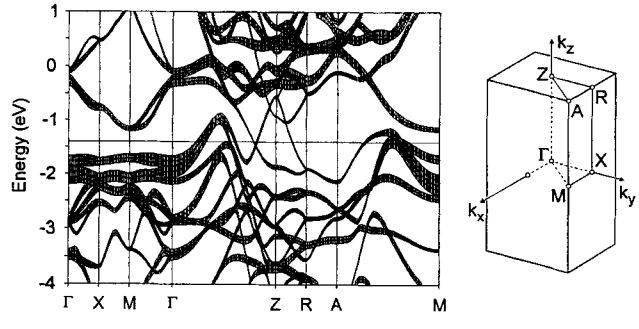

Fig. 4. Ab initio band structure of Hf_2In_5 (left) and high-symmetry points of the primitive tetragonal Brillouin zone (right). The one-electron bands are artificially widened in order to reflect their degree of hafnium character.

Since the fat hafnium-centered bands remain fairly flat in the two-dimensional regime ($\Gamma \rightarrow X \rightarrow M \rightarrow \Gamma$), the covalent part of the chemical bonding of hafnium in the *ab* plane must be negligible here. Also, there is a semiconductor-like band gap of about 0.5 eV only in this two-dimensional plane. The metallic character of Hf_2In_5, however, arises from the overlap of (fat) hafnium bands and (narrow) indium bands along the $\Gamma \rightarrow Z$ direction,

0947-6539/96/0207-0802 $ 15.00+.25/0 Chem. Eur. J. 1996, 2, No. 7

paralleling the short real-space c axis. We note that the largest dispersion of the Hf bands (also visible from the reciprocal A → M vector), and thus the strongest bonding interaction of hafnium, must also occur along this axis. In contrast, the bonding interactions in the indium sublattice seem to be preferentially directed at right angles to this axis. For example, there is a very thin, almost completely indium-centered sp band crossing the Fermi level between Z → R with a large dispersion; this indicates that indium–indium interactions are mostly located in the real-space *ab* plane, in sharp contrast to those of the hafnium atoms.

For a more quantitative bonding analysis, we now turn to the semiempirical crystal orbital overlap population (COOP) curves (Fig. 5), which allow a discussion of the space-averaged energy resolution. Based on the Hf–Hf overlap population (top), the Fermi level is in a perfect position to distinguish between bonding and antibonding interactions. We thus may assume that Hf–Hf bonding plays the dominant role in stabilizing this particular crystal structure. Anticipating results to come (see below), a charge-density analysis is in full agreement with this.

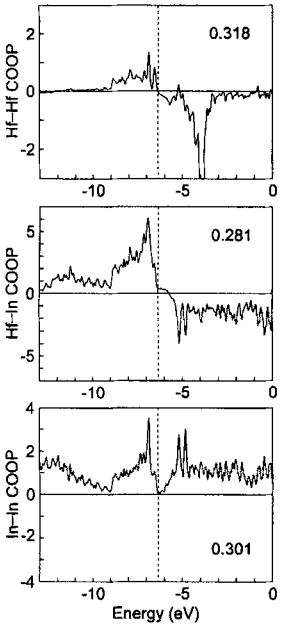

Fig. 5. Chemical bonding from semiempirical crystal orbital overlap populations (COOP) for various bonding contributions in Hf_2In_5. The averaged overlap populations of the atomic contacts Hf–Hf (≤310 pm), Hf–In (≤320 pm), and In–In (≤340 pm) are shown. The numbers represent the integrated values of the overlap populations per bond integrated up to the Fermi level.

With respect to In–In bonding (Fig. 5, bottom), the Fermi level (ε_F) also falls into a practically zero COOP minimum, but it now separates occupied bonding from unoccupied bonding contributions. If it were not for the strongly antibonding Hf–Hf interactions beyond ε_F, one might expect that Hf_2In_5 could be easily reduced, for example, by electrochemical means.

Only the covalent part of Hf–In bonding (Fig. 5, middle) shows an unoptimized shape at the Fermi level. Reiterating the above-mentioned significant charge transfer between hafnium and indium and their at least partially electrostatic mutual bonding character, we thus conclude that Hf–In covalency plays only a subordinate role inside Hf_2In_5.

All the above findings concerning the amount of interatomic bonding and their spatial preferences may be visualized by means of theoretical full-potential valence charge density plots (LMTO), given in Figures 6a and 6b.

Figure 6a shows the valence charge density in the tetragonal *ab* plane at $z = 0$, containing only the indium atoms (cf. perspective view in Fig. 1). Indeed, there is a significant residual electron density between all indium atoms, that is, between all triangular and square-planar units. Most strikingly, the additional charge density is *not* found on the direct interatomic vectors, but at positions that are more shifted towards the centers of the prisms; this demonstrates unambiguously the multicentered nature of the indium–indium bonding. Thus, Figure 6a shows that two-dimensional bonding operates in a polymeric indium

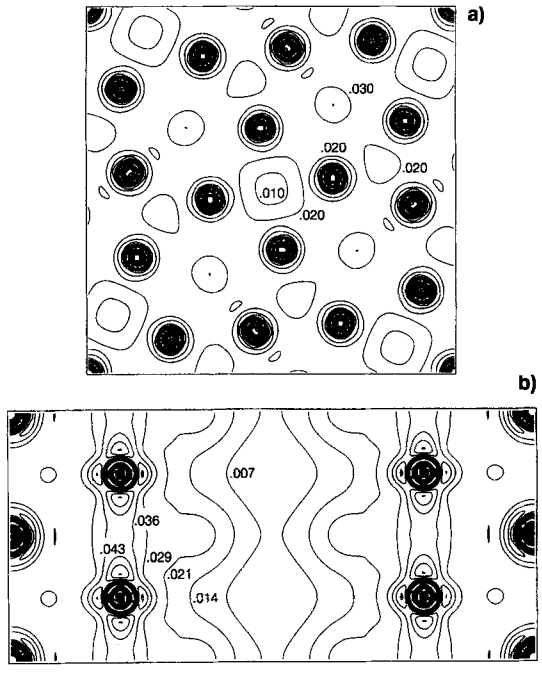

Fig. 6. Computed valence charge densities in Hf_2In_5 from first principles: a) the *ab* plane at $z = 0$ and b) a diagonal cut through the structure (see dashed line in Fig. 1) with the c axis in the vertical direction. The steps are given in units of e/a_0^3 (a_0 is the Bohr radius of about 52.9 pm).

network. We have already anticipated bonding of this type from the Z → R progression of a given indium sp band in Figure 4.

Figure 6b represents a valence charge density for a specific cut through the crystal structure (cf. dashed line in Fig. 1), containing four hafnium and six indium (edge) atoms and with the c axis running in the vertical direction. Two observations are of interest here: First, there is no residual electron density between the outer In(2) atoms although their internuclear distances (306 pm) are the shortest ones(!) in the structure. Also, the shape of the In(2) atoms does not deviate substantially from an almost perfect sphere, as would be required for any directed chemical bonding. In other words, any attempt to link interatomic distances to bond orders is destined to fail for the present case, in which there are indium–indium bonds in the *ab* plane, but not perpendicular to it, along the shorter indium–indium contacts parallel to c. Second, there are strong bonds between neighboring hafnium atoms, as can be seen from the size of the internuclear charge densities; this confirms the bond-length analysis put forward at the beginning of this paper. A detailed semiempirical orbital analysis shows that this bonding exhibits almost pure σ character in which bonding d_{z^2}–d_{z^2} and antibonding s–p_z contributions almost cancel each other. The net bond strength, however, arises from additional s–d_{z^2} (stronger) and s–s (weaker) metal–metal interactions. Referring back to Figure 6a, the charge density of these Hf–Hf bonds may also be readily perceived from the residual electron density inside the indium pentagons, which are threaded by the Hf chains.

In summary, chemical bonding in the intermetallic phase Hf_2In_5 does not follow a naive "metallic bond" or "electron gas" description; there is clear separation into positively charged two-dimensional indium networks, threaded by negatively charged one-dimensional hafnium chains.

Chemical and Physical Properties: Powders of Hf_2In_5 are dark gray and stable in air over months. No decomposition whatsoever is observed. Single crystals are light gray with a metallic

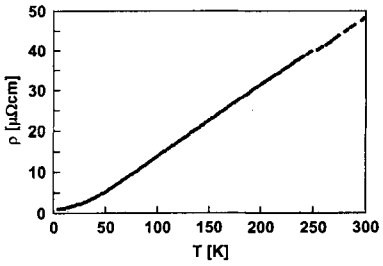

Fig. 7. Temperature dependence of the specific resistivity of Hf_2In_5.

luster, and they crystallize as needles with lengths of up to about 200 μm. Single crystals show no reaction with water, but they slowly dissolve in dilute hydrochloric acid.

The magnetic susceptibility of Hf_2In_5 shows very weak temperature-independent paramagnetism with a room-temperature value of $2.0(1) \times 10^{-5}$ emu mol^{-1}, indicative of Pauli paramagnetism.

The specific resistivity decreases with decreasing temperature (Fig. 7), as is usually observed for metallic conductors. The room-temperature value of 50 μΩcm is of the same order of magnitude as for Ti_2In_5.[17] Compared with hafnium (ρ = 32.5 μΩcm at 293 K)[48] and indium (ρ = 8.37 μΩcm at 293 K),[48] Hf_2In_5 shows good metallic conductivity.

Acknowledgements: We thank Prof. Dr. Arndt Simon for his interest in and unwavering support for this work, as well as for constructive discussions. We are also indebted to Willi Röthenbach for recording the Guinier powder patterns, to Nicola Rollbühler for the resistivity measurement, to Eva Brücher and Dr. R. K. Kremer for the susceptibility measurement, and to the Stiftung Stipendienfonds des Verbandes der Chemischen Industrie for a Liebig grant to R. P.

Received: December 1, 1995 [F259]

[1] S. C. Sevov, J. D. Corbett, *Inorg. Chem.* **1991**, *30*, 4875.
[2] S. C. Sevov, J. D. Corbett, *Inorg. Chem.* **1992**, *31*, 1895.
[3] G. Cordier, V. Müller, *Z. Kristallogr.* **1992**, *198*, 302.
[4] G. Cordier, V. Müller, *Z. Kristallogr.* **1993**, *205*, 306.
[5] S. C. Sevov, J. D. Corbett, *J. Solid State Chem.* **1993**, *103*, 114.
[6] W. Blase, G. Cordier, V. Müller, U. Häußermann, R. Nesper, M. Somer, *Z. Naturforsch.* **1993**, *48b*, 754.
[7] G. Cordier, V. Müller, *Z. Naturforsch.* **1994**, *49b*, 721.
[8] G. Cordier, V. Müller, *Z. Naturforsch.* **1995**, *50b*, 23.
[9] R. Thümmel, W. Klemm, *Z. Anorg. Allg. Chem.* **1970**, *376*, 44.
[10] W. J. A. Maaskant, *New J. Chem.* **1993**, *17*, 97.
[11] R. Dronskowski, *Inorg. Chem.* **1994**, *33*, 6201.
[12] R. Dronskowski, *Angew. Chem.* **1995**, *107*, 1230; *Angew. Chem. Int. Ed. Engl.* **1995**, *34*, 1126.
[13] R. Dronskowski, *Chem. Eur. J.* **1995**, *1*, 118.
[14] K. Schubert, *Kristallstrukturen zweikomponentiger Phasen*, Springer, Berlin, **1964**.
[15] P. Villars, L. D. Calvert, *Pearson's Handbook of Crystallographic Data for Intermetallic Phases*, 2nd ed., American Society for Metals, Materials Park, OH 44073, **1991**.
[16] R. Pöttgen, *J. Alloys Compd.* **1995**, *226*, 59.
[17] R. Pöttgen, *Z. Naturforsch.* **1995**, *50b*, 1505.
[18] R. G. Johnson, R. J. Prosen, *Trans. Metallurg. Soc. AIME* **1962**, *224*, 297.
[19] A. Raman, K. Schubert, *Z. Metallkd.* **1965**, *56*, 44.
[20] H. L. Krauss, H. Stach, *Z. Anorg. Allg. Chem.* **1969**, *366*, 34.
[21] A. Simon, *J. Appl. Crystallogr.* **1971**, *4*, 138.
[22] K. Yvon, W. Jeitschko, E. Parthé, *J. Appl. Crystallogr.* **1977**, *10*, 73.
[23] G. M. Sheldrick, SHELXL-93, Program for Crystal Structure Refinement, University of Göttingen, Germany, 1993.
[24] Further details of the crystal structure investigation may be obtained from the Fachinformationszentrum Karlsruhe, 76344 Eggenstein-Leopoldshafen (Germany) on quoting the depository number CSD-404531.
[25] R. Hoffmann, *J. Chem. Phys.* **1963**, *39*, 1397.
[26] R. Hoffmann, *Solids and Surfaces: A Chemist's View of Bonding in Extended Structures*, VCH, Weinheim, New York, **1988**.
[27] J. H. Ammeter, H.-B. Bürgi, J. C. Thibeault, R. Hoffmann, *J. Am. Chem. Soc.* **1978**, *100*, 3686.
[28] J. P. Desclaux, *At. Data Nucl. Data Tables* **1973**, *12*, 311.
[29] P. Pykkö, L. L. Lohr, Jr., *Inorg. Chem.* **1981**, *20*, 1950.
[30] M.-H. Whangbo, M. Evain, T. Hughbanks, M. Kertesz, S. Wijeyesekera, C. Wilker, C. Zheng, R. Hoffmann, *QCPE program EHMACC*.
[31] O. K. Andersen, *Phys. Rev. B* **1975**, *12*, 3060.
[32] O. K. Andersen, O. Jepsen, D. Götzel, in *Highlights of Condensed-Matter Theory* (Eds.: F. Bassani, F. Fumi, M. P. Tosi), North-Holland, New York, **1985**.
[33] H. L. Skriver, *The LMTO Method*, Springer, Berlin, Heidelberg, New York, **1984**.
[34] O. K. Andersen, O. Jepsen, M. Sob, in *Electronic Band Structure and its Applications* (Ed.: M. Yussouf), Springer, Berlin, **1986**.
[35] J. Korringa, *Physica* **1947**, *13*, 392.
[36] W. Kohn, N. Rostoker, *Phys. Rev.* **1954**, *94*, 111.
[37] P. Hohenberg, W. Kohn, *Phys. Rev. B* **1964**, *136*, 864.
[38] W. Kohn, L. J. Sham, *Phys. Rev. A* **1965**, *140*, 1133.
[39] U. von Barth, L. Hedin, *J. Phys. C* **1972**, *5*, 1629.
[40] O. K. Andersen, O. Jepsen, *Phys. Rev. Lett.* **1984**, *53*, 2571.
[41] P. E. Blöchl, O. Jepsen, O. K. Andersen, *Phys. Rev. B* **1994**, *49*, 16223.
[42] M. van Schilfgarde, T. A. Paxton, O. Jepsen, G. Krier, A. Burkhard, O. K. Andersen, *TB-LMTO 4.6 Program*.
[43] J. F. De Wet, *Acta Crystallogr.* **1961**, *14*, 733.
[44] R. G. Pearson, *Inorg. Chem.* **1988**, *27*, 734.
[45] L. Pauling, *The Nature of the Chemical Bond and the Structure of Molecules and Crystals*, Cornell University Press, **1960**.
[46] E. Teatum, K. Gschneidner, Jr., J. Waber, Rep. *LA-2345*, 1960 (US Department of Commerce, Washington, DC).
[47] J. Donohue, *The Structures of the Elements*, Wiley, New York, **1974**.
[48] *Handbook of Chemistry and Physics* (Ed.: R. C. Weast), 66th ed., CRS Press, Florida, **1985**.

0947-6539/96/0207-0804 $ 15.00+.25/0